blood®
Regular Article

LYMPHOID NEOPLASIA

Characterization of DLBCL with a PMBL gene expression signature

Gerben Duns,[1,2,*] Elena Viganò,[1,2,*] Daisuke Ennishi,[1] Clementine Sarkozy,[1,3] Stacy S. Hung,[1] Elizabeth Chavez,[1] Katsuyoshi Takata,[1] Christopher Rushton,[4] Aixiang Jiang,[1,2] Susana Ben-Neriah,[1] Bruce W. Woolcock,[1] Graham W. Slack,[1] Eric D. Hsi,[5] Jeffrey W. Craig,[1] Laura K. Hilton,[1,4] Sohrab P. Shah,[6,7] Pedro Farinha,[1] Anja Mottok,[1,8] Randy D. Gascoyne,[1] Ryan D. Morin,[4,9] Kerry J. Savage,[1] David W. Scott,[1,†] and Christian Steidl[1,†]

[1]Centre for Lymphoid Cancer, BC Cancer, Vancouver, BC, Canada; [2]Department of Pathology and Laboratory Medicine, University of British Columbia, Vancouver, BC, Canada; [3]Early Phase Clinical Trial Department, Institut Gustave Roussy, Villejuif, France; [4]Department of Molecular Biology and Biochemistry, Simon Fraser University, Burnaby, BC, Canada; [5]Pathology and Laboratory Medicine Institute, Cleveland Clinic, Cleveland, OH; [6]Molecular Oncology and [7]Canada's Michael Smith Genome Sciences Centre, British Columbia Cancer, Vancouver, BC, Canada; [8]Institute of Human Genetics, Ulm University Medical Center, Ulm University, Ulm, Germany; and [9]Department of Medical Genetics, University of British Columbia, Vancouver, BC, Canada

KEY POINTS

- **nm-PMBLsig$^+$ tumors represent a distinct group of DLBCLs that share molecular features with bf-PMBL.**
- **Mutational patterns and anatomic presentations suggest distinct evolutionary modes between nm-PMBLsig$^+$ tumors and bf-PMBL.**

Primary mediastinal large B-cell lymphoma (PMBL) is a type of aggressive B-cell lymphoma that typically affects young adults, characterized by presence of a bulky anterior mediastinal mass. Lymphomas with gene expression features of PMBL have been described in non-mediastinal sites, raising questions about how these tumors should be classified. Here, we investigated whether these nonmediastinal lymphomas are indeed PMBLs or instead represent a distinct group within diffuse large B-cell lymphoma (DLBCL). From a cohort of 325 de novo DLBCL cases, we identified tumors from patients without evidence of anterior mediastinal involvement that expressed a PMBL expression signature (nm-PMBLsig$^+$; n = 16; 5%). A majority of these tumors expressed MAL and CD23, proteins typically observed in bona fide PMBL (bf-PMBL). Evaluation of clinical features of nm-PMBLsig$^+$ cases revealed close associations with DLBCL, and a majority displayed a germinal center B cell–like cell of origin (GCB). In contrast to patients with bf-PMBL, patients with nm-PMBLsig$^+$ presented at an older age and did not show pleural disease, and bone/bone marrow involvement was observed in 3 cases. However, although clinically distinct from bf-PMBL, nm-PMBLsig$^+$ tumors resembled bf-PMBL at the molecular level, with upregulation of immune response, JAK-STAT, and NF-κB signatures. Mutational analysis revealed frequent somatic gene mutations in *SOCS1*, *IL4R*, *ITPKB*, and *STAT6*, as well as *CD83* and *BIRC3*, with the latter genes significantly more frequently affected than in GCB DLBCL or bf-PMBL. Our data establish nm-PMBLsig$^+$ lymphomas as a group within DLBCL with distinct phenotypic and genetic features. These findings may have implications for gene expression– and mutation-based subtyping of aggressive B-cell lymphomas and related targeted therapies.

Introduction

Aggressive B-cell lymphomas account for >40% of newly diagnosed B-cell non-Hodgkin lymphoma (NHL) cases worldwide. Among these, diffuse large B-cell lymphoma (DLBCL) is by far the most common. It is a biologically and clinically heterogeneous disease that shows a wide range of clinical outcomes after standard treatments, highlighting the need to accurately define molecular subgroups that have prognostic significance and harbor potentially targetable biology.[1]

In contrast, primary mediastinal large B-cell lymphoma (PMBL) represents a relatively rare subtype, accounting for 2% to 3% of B-cell NHLs. It typically affects young adults, with a higher frequency in women, and is characterized by the presence of a bulky anterior mediastinal mass.[2] Based on its anatomic location and immunophenotypic signature, PMBL has been postulated to be derived from thymic medullary B cells.[3,4] Although its morphologic features are mostly reminiscent of DLBCL,[5] gene expression (GE) profile analyses have shown that PMBL is more closely related to classic Hodgkin lymphoma (cHL).[6,7] This relationship to cHL was further corroborated by recent studies that revealed frequent aberrations affecting immune response, JAK-STAT, and NF-κB signaling, representing molecular findings distinct from DLBCL but similar to cHL.[8,9]

PMBL has been recognized as a distinct lymphoma entity in the World Health Organization classification since 2001, but its diagnosis is, in most cases, still based on clinicopathologic consensus. In

particular, the lack of histologic features that reliably distinguish PMBL from other types of B-cell NHL that may involve mediastinal lymph nodes can make a definitive diagnosis challenging.[10] GE profiling has been shown to accurately differentiate PMBL from DLBCL with mediastinal involvement, but despite some translational efforts, diagnostic GE-based tests have not yet entered routine clinical practice.[6,7,11,12]

Yuan et al[13] reported the identification of PMBL tumors observed at nonmediastinal sites. These tumors were initially diagnosed as DLBCL and showed no evidence of mediastinal involvement but expressed a PMBL-like signature. However, compared with PMBL tumors with anterior mediastinal involvement, they had significantly fewer aberrations involving *CIITA* or *PDL1*/*PDL2*. Patients with PMBL tumors without apparent mediastinal involvement were older, and there was more equal sex distribution compared with those with mediastinal PMBL. However, these differences did not reach statistical significance, likely reflecting a small sample size. Therefore, whether "nonmediastinal PMBLs" (nm-PMBLsig$^+$) are indeed PMBLs or alternatively represent a distinct subtype of DLBCL remains an open question.

Methods

Patient cohorts

To enhance our understanding of the subset of DLBCL that exhibits a PMBL GE signature, we analyzed the mutational and clinical characteristics of 325 de novo tumors with DLBCL morphology, treated with rituximab plus cyclophosphamide, doxorubicin, vincristine, and prednisone (R-CHOP), selected from the BC Cancer (BCC) population-based registry. All DLBCL cases had *MYC*, *BCL2*, and *BCL6* fluorescence in situ hybridization, RNA sequencing (RNAseq), OncoSNP copy-number (CN) call, and targeted capture sequencing results available from previously published studies.[14,15]

Mutational frequencies and clinical characteristics of nm-PMBLsig$^+$ tumors were compared with those of bona fide PMBLs (bf-PMBLs) that were part of a previously described PMBL cohort drawn from the BCC population-based registry and centrally reviewed by the pathologist panel of the Lymphoma/Leukemia Molecular Profiling Project.[11]

This work was reviewed and approved by the University of British Columbia–BC Cancer Research Ethics Board in accordance with the Declaration of Helsinki.

DLBCL90 NanoString assay

The DLBCL90 NanoString subtyping assay for aggressive B-cell lymphoma was applied to 325 DLBCL samples to identify tumors with the PMBL GE signature, assign cell-of-origin (COO) group, and determine double-hit signature (DHITsig) status.[11,16] Linear predictor scores and empiric Bayesian probabilities[17] were calculated for all samples using the DLBCL90 R package.

IHC staining

Immunohistochemical staining (IHC) was performed on tissue microarrays, comprising cores from the diagnostic biopsies of the cohort, using antibodies and thresholds described in supplemental Table 1, available on the *Blood* Web site.

WES

Whole-exome sequencing (WES) was performed on 15 fresh frozen nm-PMBLsig$^+$ tumors and 7 matched normal samples. Genomic libraries were prepared using the SureSelectXT Target Enrichment System for Illumina Paired-End Multiplexed Sequencing Library protocol and 200 ng of input genomic DNA. Each indexed library was then hybridized to the SureSelect Human All Exon V6+UTR capture library and sequenced on an Illumina NextSeq550 using 150-bp paired-end reads. Tumor and normal DNA samples were sequenced to an average depth of 117× (standard deviation, 30×). All reads were aligned to the human reference genome using bwa-mem (version 0.7.5a)[18] with optical and polymerase chain reaction duplicates removed using the Picard tool (http://broadinstitute.github.io/picard/).

WES analysis

Somatic single-nucleotide variant (SNV)/indel variants were identified using the intersection of calls predicted by VarScan (version 2.3.6),[19] Strelka (version 1.0.13),[20] and MuTect (version 1.1.4).[21] All variants were annotated using SnpEff (version 4.2)[22] and filtered for effects predicted to have an impact at the protein level (nonsynonymous, stop gained, and splice site). Variants were filtered for a minimum of 3 variant reads, 10% variant allele frequency, and global minor allele frequency <1%. Unpaired tumors (n = 8) were matched against a pooled normal that was constructed from normal samples for paired tumors (n = 7). Variants from unpaired tumors were further filtered to remove potential germline single-nucleotide polymorphisms if the variant was present in dbSNP (version 137)[23] but not COSMIC (version 68).[24]

Mutation calls from an external DLBCL cohort

Mutational frequencies in nm-PMBLsig$^+$ tumors assessed by WES were compared with mutational frequencies observed in DLBCLs from Schmitz et al,[25] who excluded cases with a PMBL signature from their study cohort. Germinal center B cell–like (GCB) DLBCLs were selected using the gene expression subgroup annotation that was based on RNAseq data. Variant calls were obtained using MuTect2[21] and postfiltered to remove germline and low-confidence variants as described in the supplemental Data.

GE analysis

RNAseq library construction and STAR alignment procedures have been described previously.[26] Gene-level read counts were quantified using HTSEQ-count (intersection strict, reverse mode).[27] Raw read counts were normalized and scaled using trimmed mean of M-values normalization and $\log_2$-transformed counts-per-million scaling, respectively.[28]

CN analysis from WES data

CN alterations in nm-PMBLsig$^+$ and bf-PMBL tumors were called from WES data using CNVkit (version 0.9.1)[29] with default thresholds. To identify relevant regions of CN alterations, GISTIC (version 2.0)[30] was applied to the curated segmentation results. The supplemental Data provides a detailed description.

IL-4 receptor expression, site-directed mutagenesis, and reporter gene assays in HEK293-STAT6 cells

IL4R mutations were created using the GENEART site-directed mutagenesis system (Thermo Fisher Scientific) according to the manufacturer's instructions. Wild-type (WT) *IL4R* and mutants were cloned into pcDNA3.1, and empty pcDNA3.1 was used as

a mock vector. The plasmids were purified using the Spin Miniprep Kit (Qiagen), and 1 μg of plasmid was transfected into HEK293 cells expressing STAT6 (HEK293 interleukin-4 [IL-4]/IL-13; Invivogen), seeded the day before at 0.25×10^6 cells per well (12 multiwell plates) using Lipofectamine2000 (Invitrogen). Twenty-four hours after transfection, cell-free supernatants were collected to assess the secreted embryonic alkaline phosphatase levels according to the manufacturer's protocol, and cells were lysed for immunoblotting analysis.

Preparation of doxycycline-inducible cell lines, retroviral transduction, and cell culture

Retroviral transduction of DEV cells was performed as previously described.[31] Briefly, DEV cells were first transduced with a feline endogenous virus (FEV) expressing the ecotropic retroviral receptor (DEV-FEV). DEV-FEV cells were secondarily infected with a retrovirus expressing the bacterial tetracycline repressor, after which they were infected with retroviral particles containing the inducible vector pRETRO-TO-PuroGFP (donated by Louis M. Staudt, National Cancer Institute, Bethesda, MD), in which the cytomegalovirus promoter is used to drive expression of cloned WT *IL4R* or mutants in the presence of 20 ng/mL of doxycycline (Sigma-Aldrich). Stable GFP^+ cells were sorted using BD FACSAria Fusion. Transduced DEV cells were cultured in RPMI 1640–GlutaMAX medium (Gibco) supplemented with 20% fetal bovine serum in the presence of doxycycline (20 ng/mL).

Western blotting and flow cytometry

Western blotting and flow cytometry were performed as previously described.[31] Briefly, membranes were probed with the following primary antibodies at 1:1000 dilution ratio unless stated otherwise: phosphorylated STAT6 (pSTAT6; 9364; Cell Signaling Technology), STAT6 (ab32108; Abcam), and IL4 receptor (IL4R; sc-28361; 1:500; Santa Cruz Biotechnology). Glyceraldehyde-3-phosphate dehydrogenase (MAB374; 1:5000; Millipore) antibody was used as internal control. Bands were visualized using the enhanced chemiluminiscence system (GE Healthcare) on a Chemidoc digital imager (Bio-Rad), and intensities of bands were quantified using Image Laboratory software (Bio-Rad). Flow cytometric analysis for surface expression of IL4R (CD124) was performed using an LSRFortessa (Becton-Dickinson Biosciences).[31]

Quantitative reverse transcription polymerase chain reaction

Total RNA was isolated using the RNeasy Kit (Qiagen) and treated with DNAse I (Promega). *CCL17* (Hs00171074_m1) and *CD23* (Hs01077044_m1) TaqMan GE Assay probes were used to detect messenger RNA levels as previously described.[31]

Statistical analysis

For the comparison of baseline clinical characteristics of patients between lymphoma subsets, data were tested by Wilcoxon rank sum (continuous data) or χ^2 (Pearson χ^2) test (categorical data). A Fisher's exact test was used to compare frequencies of mutations and IHC scores between lymphoma subsets. All analyses were performed using R software (version 3.6.3; https://cran.r-project.org/src/base/R-3/) For in vitro experiments, comparisons between groups were performed using a 2-sample Student *t* test, (GraphPad Prism 8).

Results

Identification of tumors with DLBCL morphology expressing a PMBL signature

The recently developed DLBCL90 NanoString assay was designed to classify tumors based on COO[32] and identify those with a PMBL[11] or DHIT[16] GE signature. We applied the DLBCL90 assay, following the 3-tiered classification system depicted in Figure 1A, to 325 diagnostic biopsy samples of patients with de novo DLBCL treated with R-CHOP.[26,33] Nineteen tumors (5.8%) were found to have a PMBL GE signature ($PMBLsig^+$) (Figure 1B). This assignment was supported by RNAseq analysis that showed strong expression of PMBL signature genes published by Rosenwald et al[6] (supplemental Figure 1). The remaining tumors were classified as $DHITsig^+$ DLBCL (n = 66 samples; 20.3% of total), GCB DLBCL (n = 110; 33.8%), unclassified DLBCL (n = 32; 9.8%), or activated B-cell (ABC) DLBCL (n = 98; 30.2%).

Clinical characteristics of nonmediastinal B-cell NHLs with a PMBL GE signature

The 19 tumors that expressed a PMBL GE signature were rereviewed by an expert panel of pathologists, radiologists, and oncologists. In 3 cases, the clinicopathologic features were deemed to be compatible with a diagnosis of PMBL; these cases were subsequently excluded from further analysis (Figure 1B). We then comprehensively characterized the clinicopathologic and genomic features of the remaining 16 tumors that did not show mediastinal involvement but expressed the PMBL GE signature ($nm\text{-}PMBLsig^+$) and compared the findings with those of the remaining DLBCL cohort, as well as with a collection of bf-PMBLs published previously.[8]

From a clinical point of view, patients with $nm\text{-}PMBLsig^+$ tumors were similar to those from the remaining DLBCL cohort but differed markedly from those with bf-PMBL (Table 1). Patients with $nm\text{-}PMBLsig^+$ tumors were significantly older than those with bf-PMBL (median age at diagnosis, 66 vs 33 years; $P < .001$), and fewer presented with elevated serum lactate dehydrogenase levels or B symptoms (44% vs 78%; $P = .006$ and 19% vs 81%; $P < .001$, respectively). Pleural and/or pericardial effusions were rarely observed in patients with $nm\text{-}PMBLsig^+$ tumors but were prevalent in patients with bf-PMBL (6% vs 30%; $P = .045$ and 0% vs 36%; $P < .001$, respectively). Involvement of bone marrow, which is highly unusual in bf-PMBL, was observed in 3 $nm\text{-}PMBLsig^+$ cases (19% vs 0%; $P < .001$).

Translocations affecting *MYC*, *BCL2*, and *BCL6* were found in 4 (25%), 5 (33%), and 2 (13%) $PMBLsig^+$ tumors, respectively (Figures 2 and 3A). Three $PMBLsig^+$ tumors were found to be HGBL-DH/TH. The results presented in the main article text reflect analyses including both DLBCL not otherwise specified (DLBCL, NOS) and HGBL-DH/TH, whereas analyses in the data supplement are restricted to DLBCL, NOS. All $PMBLsig^+$ tumors were Epstein-Barr virus negative (Figure 2) and did not reveal structural rearrangements affecting *CIITA*, as assessed by a breakapart fluorescence in situ hybridization assay (S.B.-N.; data not shown). The vast majority of $nm\text{-}PMBLsig^+$ tumors had a GCB GE signature, compared with approximately half of the remaining DLBCLs (88% vs 56%; $P = .01$; Table 1; Figure 1B).

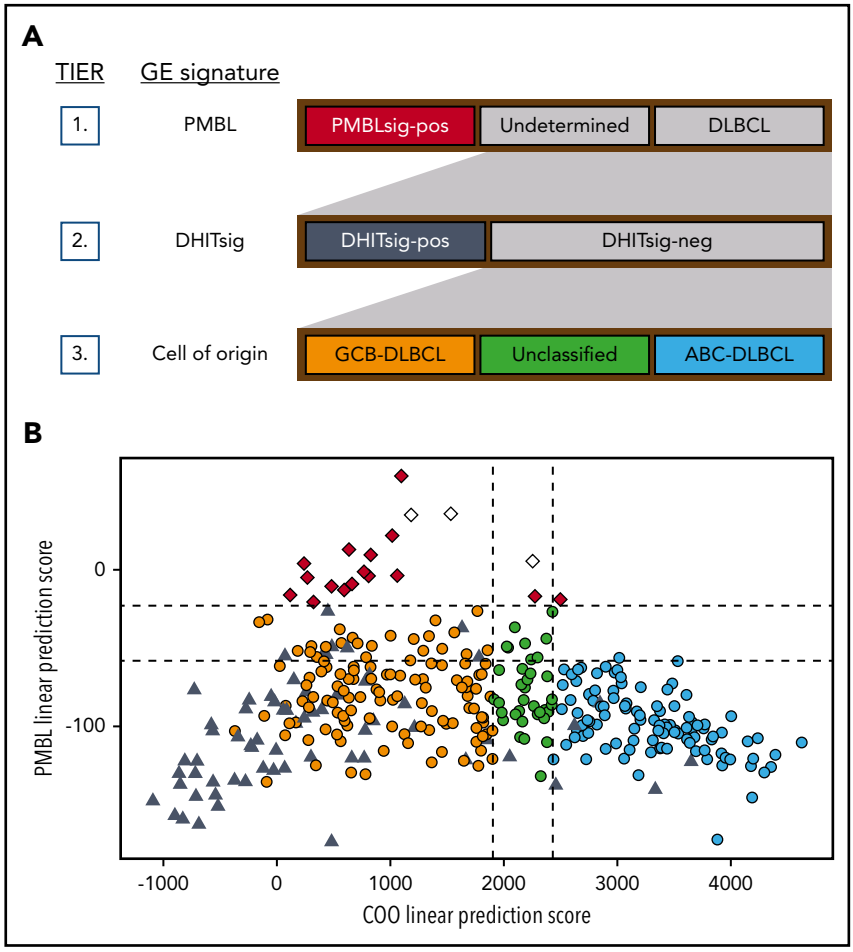

Figure 1. DLBCL90 assay: tiered classification system and scores. (A) Tiered classification of DLBCL tumors using the DLBCL90 NanoString assay. Tier 1: in the first layer of this 3-tiered classification system, PMBLsig$^+$ samples are identified. Tier 2: DHITsig$^+$ samples are then identified among the samples that do not have a PMBL GE signature. Tier 3: in the final tier, the remaining samples are categorized based on their COO. (B) DLBCL90 assay scores for 325 de novo DLBCL tumors from the BCC DLBCL cohort. PMBL linear prediction scores (LPSs) are plotted against COO LPSs for each sample. Low COO LPS result in an assignment to the GCB group, whereas high LPS result in an activated B-cell (ABC) assignment. High PMBL LPS results in an assignment to the PMBLsig$^+$ group. Dotted lines represent the cutoffs between categories. Red, PMBLsig$^+$; orange, GCB; green, unclassified; blue, ABC; black, DHITsig$^+$; white, samples from patients found to have presented with bf-PMBL–like features and who were therefore excluded from further analysis.

nm-PMBLsig$^+$ tumors and bf-PMBL share a common immunophenotype

All PMBLsig$^+$ tumors showed similar morphologic features on hematoxylin and eosin stain, with abundant eosinophilic cytoplasm, resembling the typical morphology of PMBL tumor cells. A majority of nm-PMBLsig$^+$ tumors stained positive for PMBL markers CD23 (71%) and MAL (57%), whereas detectable expression of these proteins was rare or absent within the rest of the DLBCL cohort (9% and 0%, respectively; $P < .001$).[34,35] Four nm-PMBLsig$^+$ tumors (25%) stained positive for programmed death ligand 1 (PDL1) and/or PDL2, compared with 12 other DLBCLs (4%; $P < .001$). None of the PMBLsig$^+$ tumors showed loss of FAS staining, compared with 35% of the other DLBCLs ($P = .02$). The GCB COO of the PMBLsig$^+$ tumors was confirmed by IHC staining for CD10, BCL6, and MUM, followed by application of the Hans algorithm[36] (Figure 2; supplemental Tables 2 and 3). Analysis of the cohort without HGBL-DH/TH tumors revealed a similar picture, showing positive staining of CD23, MAL, PDL1/2, and FAS to be prominently enriched among PMBLsig$^+$ tumors (supplemental Figure 2; supplemental Table 4).

Mutational analysis of nm-PMBLsig$^+$ tumors confirms molecular commonalities with bf-PMBL but suggests different modes of immune evasion

We performed WES on the 15 nm-PMBLsig$^+$ tumors for which DNA was available. We identified, on average, 276 (range, 26-440) somatic nonsynonymous mutations with a variant allele frequency of at least 5% (supplemental Table 5; supplemental Figure 3). We then compared the mutational landscape of these nm-PMBLsig$^+$ samples with the mutational patterns observed in 73 bf-PMBLs.[8]

Notably, all nm-PMBLsig$^+$ tumors showed ≥1 mutation affecting genes encoding proteins involved in JAK-STAT signaling, including *SOCS1*, *DUSP2*, *IL4R*, and *STAT6*, akin to those found in bf-PMBL[8,9] (Figures 3A-B and 4A).

Mutations affecting *BIRC3*, which encodes an E3 ubiquitin ligase involved in NF-κB signaling,[37] were highly enriched in nm-PMBLsig$^+$ tumors compared with bf-PMBL (Figure 3A-C; supplemental Figure 4A). The *BIRC3* p.Leu548X frameshift mutation, identified in 1 nm-PMBLsig$^+$ tumor, is similar to the mutations that are frequent in mantle cell lymphoma and that invariably truncate the BIRC3 RING domain, resulting in loss of its ubiquitinating capacity (supplemental Figure 7).[38-40] In 2 samples, we identified mutations affecting the BIR3 domain: an in-frame 9-bp deletion and a missense mutation categorized as highly likely to be damaging to the protein. The final *BIRC3* mutation, a p.Gln515His missense mutation, affects the CARD domain, which is required for BIRC3 autoregulation.[41] The recurrent aberrations affecting *BIRC3* and *NFKBIE* identified in nm-PMBLsig$^+$ tumors and bf-PMBL,[8,42] respectively, suggest that although perturbation of NF-κB signaling is common in both entities, this disruption is most often established through distinct mechanisms (Figures 3A-C and 4B). In a similar fashion, mutations affecting immune response were prevalent in both nm-PMBLsig$^+$ tumors (*CD83*) and bf-PMBL

Table 1. Baseline clinical characteristics of patients with nm-PMBLsig$^+$ tumors, other DLBCLs, or bf-PMBL

Characteristic	Other DLBCLs (n = 306)		nm-PMBLsig$^+$ (n = 16)		bf-PMBL (n = 73)
	n (% of total)	*P**	n (% of total)	*P*†	n (% of total)
Age, y		.42		**<.001**	
Median	64		66		33
Range	16-92		19-80		13-58
Sex		.26		.41	
Male	196 (64)		8 (50)		29 (40)
Female	110 (36)		8 (50)		44 (60)
ECOG PS		.54		.45	
≤1	205 (68)		12 (75)		47 (65)
>1	98 (32)		4 (25)		25 (35)
Unknown	3		—		1
Serum LDH level		.51		**.006**	
Normal	134 (48)		9 (56)		16 (22)
Elevated	146 (52)		7 (44)		57 (78)
Unknown	26		—		—
Ann Arbor stage		.50		.13	
I/II	144 (48)		9 (56)		54 (75)
III/IV	159 (52)		7 (44)		18 (25)
Unknown	3		—		1
B symptoms		.12		**<.001**	
Absent	187 (62)		13 (81)		14 (19)
Present	115 (38)		3 (19)		58 (81)
Unknown	4		—		1
IPI		.78		.50	
0-2	192 (65)		11 (69)		51 (75)
>2	102 (35)		5 (31)		17 (25)
Unknown	12		—		5
Bulky disease (≥10 cm)		.08		**<.001**	
No	219 (74)		15 (94)		39 (46)
Yes	77 (26)		1 (6)		28 (54)
Unknown	10		—		1
COO (Lymph2Cx)		**.012**		.40	
GCB	170 (56)		14 (88)		57 (78)
Non-GCB	136 (44)		2 (13)		16 (22)
No. of identified extranodal sites		.38		**.007**	
0 or 1	261 (86)		15 (94)		28 (51)
≥2	42 (14)		1 (6)		27 (49)
Unknown	3		—		18
Involvement of extranodal sites of interest					
Bone marrow		.43		**<.001**	
Not identified	269 (88)		13 (81)		73 (100)
Identified	37 (12)		3 (19)		0 (0)
Pericardial effusion		.82		**.004**	
Not identified	305 (100)		16 (100)		47 (64)
Identified	1 (0)		0 (0)		26 (36)

Bold *P* values indicate significance.

ECOG PS, Eastern Cooperative Oncology Group performance status; IPI, International Prognostic Index; LDH, lactate dehydrogenase.

*Compared with other DLBCLs using the Wilcoxon rank sum test for continuous data (age) and χ^2 (Pearson χ^2 test) for categorical data.

†Compared with bf-PMBL using the Wilcoxon rank sum test for continuous data (age) and χ^2 (Pearson χ^2 test) for categorical data.

Table 1. (continued)

Characteristic	Other DLBCLs (n = 306)		nm-PMBLsig$^+$ (n = 16)		bf-PMBL (n = 73)
	n (% of total)	*P**	n (% of total)	*P*†	n (% of total)
Pleural effusion		.52		.045	
Not identified	296 (97)		15 (94)		51 (70)
Identified	10 (3)		1 (6)		22 (30)
Lung		.08		.33	
Not identified	295 (96)		14 (88)		56 (77)
Identified	11 (4)		2 (12)		17 (23)

Bold *P* values indicate significance.

ECOG PS, Eastern Cooperative Oncology Group performance status; IPI, International Prognostic Index; LDH, lactate dehydrogenase.

*Compared with other DLBCLs using the Wilcoxon rank sum test for continuous data (age) and χ^2 (Pearson χ^2 test) for categorical data.

†Compared with bf-PMBL using the Wilcoxon rank sum test for continuous data (age) and χ^2 (Pearson χ^2 test) for categorical data.

(*B2M* and *CIITA*), but the differences in the specific genes involved suggest distinct mechanisms of immune evasion (Figures 3A-C and 4C).[43,44]

IL4R mutation patterns and function differ significantly between nm-PMBLsig$^+$ tumors and GCB DLBCL

Several of the frequently mutated genes in nm-PMBLsig$^+$ tumors, including those affecting JAK-STAT genes and *CD83*, were found to be mutated in far lower fractions or were absent in GCB DLBCL (Figures 3B,D and 4A-C; supplemental Figure 4B).

In addition, analysis of the targeted sequencing results from the BCC DLBCL cohort[15,26] revealed that *IL4R* mutations were more frequent in nm-PMBLsig$^+$ tumors compared with GCB DLBCL (supplemental Figure 5), and the *IL4R* mutational patterns were different. While the previously reported transmembrane hotspot mutation p.I242N[31] was present in both nm-PMBLsig$^+$ tumors and GCB DLBCL, nm-PMBLsig$^+$ samples showed an enrichment of mutations affecting the extracellular domain and less frequent cytoplasmic mutations compared with GCB DLBCL (Figure 5A).

In vitro experiments showed that mutations affecting the extracellular domain of IL4R (p.N151I, p.Y225, and p.F229C) had the ability to constitutively activate the downstream JAK-STAT pathway, similarly to p.I242N.[31] In contrast, mutations affecting the cytoplasmic domain of IL4R did not lead to JAK-STAT pathway activation. Upon ectopic expression of IL4R with extracellular

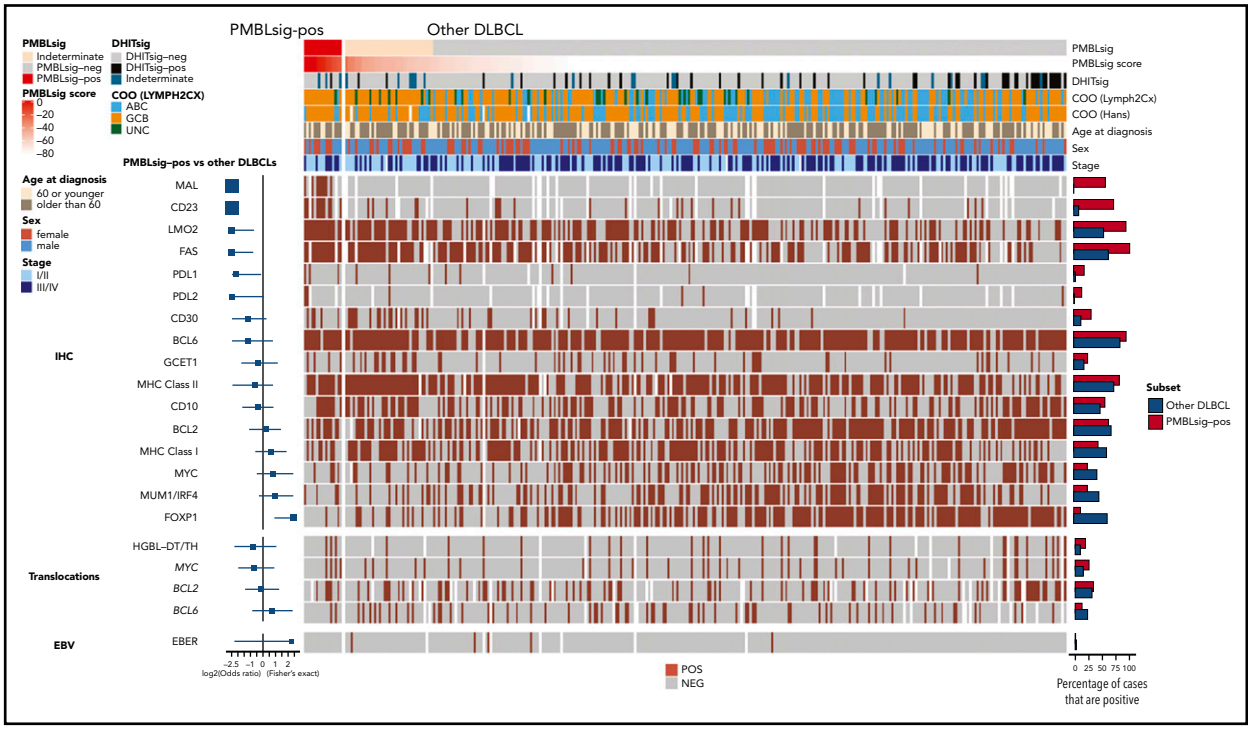

Figure 2. Immunophenotypic characteristics and translocation status of PMBLsig$^+$ tumors and other tumors with DLBCL morphology. Forest plots at the left show enrichment or depletion of positive tumors among the PMBLsig$^+$ group compared with other DLBCLs for each marker/translocation. Bar plots at the right represent the fraction of cases positive for each marker/translocation. ABC, activated B-cell–like; EBV, Epstein-Barr virus; HGBL-DH/TH, high-grade B-cell lymphoma with *MYC* and *BCL2* and/or *BCL6* rearrangement; MHC, major histocompatibility complex; UNC, unclassified.

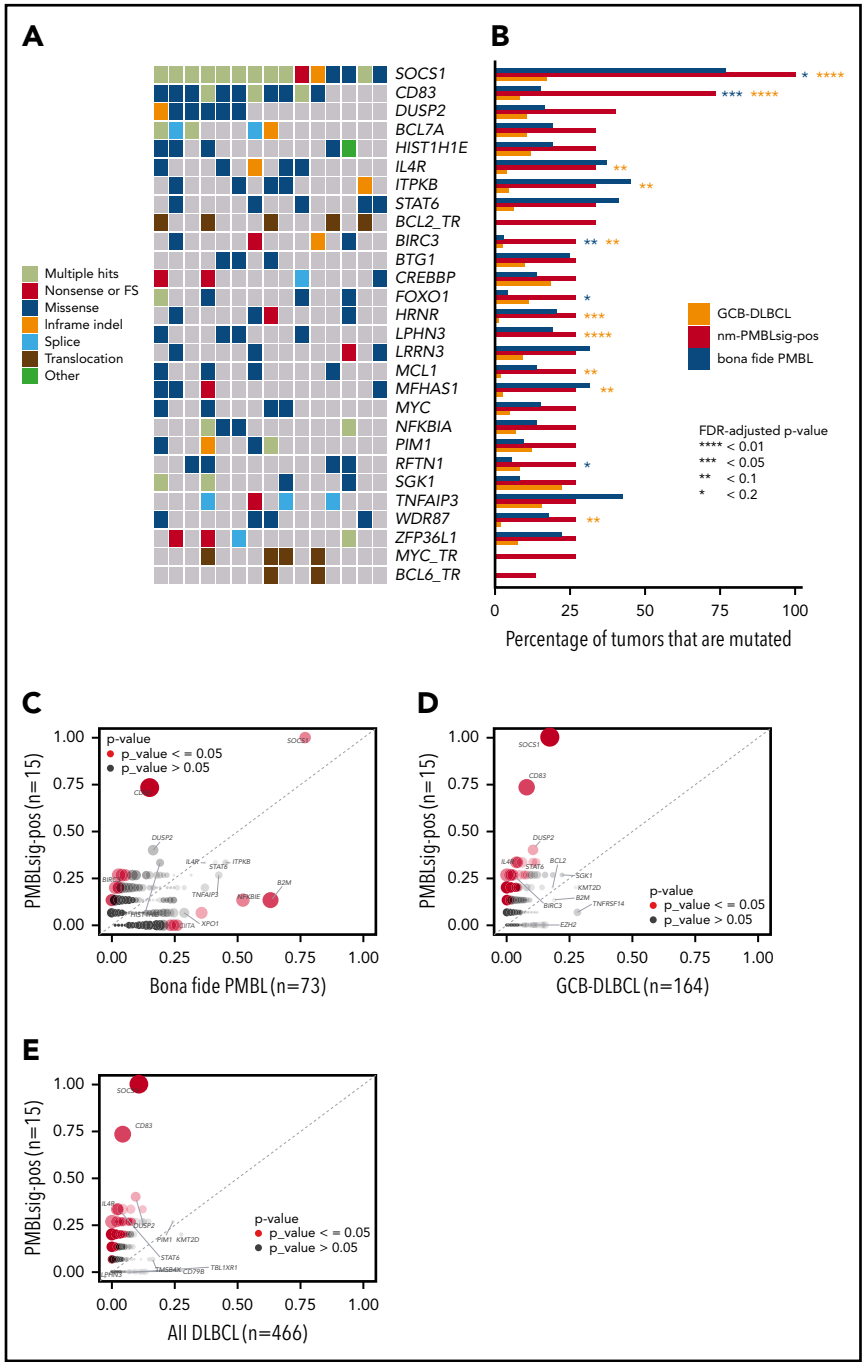

Figure 3. Mutational landscape of nm-PMBLsig⁺ tumors. (A) Oncoplot showing the somatic mutational landscape of nm-PMBLsig⁺ tumors. Genes mutated in at least 4 nm-PMBLsig⁺ tumors (≥27%) and translocations affecting *MYC*, *BCL2*, and *BCL6* are shown. Colors represent various mutation types, as indicated. (B) Mutational frequency of selected genes in nm-PMBLsig⁺ tumors, GCB DLBCL, and bf-PMBL. Mutational frequencies of genes depicted in panel A are shown for nm-PMBLsig⁺ tumors (BCC DLBCL cohort), GCB DLBCL (Schmitz/Staudt cohort), and bf-PMBL (BCC PMBL cohort). Purple and orange asterisks represent significance of enrichment of mutations in nm-PMBLsig⁺ tumors vs bf-PMBL and nm-PMBLsig⁺ tumors vs GCB DLBCL, respectively (Fisher's exact test). *MYC*, *BCL2*, and *BCL6* translocation status was not assessed or has not been reported for the bf-PMBL and DLBCL samples from the Schmitz cohort. (C-E) Mutational enrichment plots showing mutational frequencies per gene in nm-PMBLsig⁺ tumors vs bf-PMBL (C), nm-PMBLsig⁺ tumors vs GCB DLBCL (D), and nm-PMBLsig⁺ vs all DLBCLs (E). Size and opacity of the data points are proportional to the significance of enrichment or depletion of the number of mutations affecting a given gene in nm-PMBLsig⁺ samples compared with bf-PMBL (C), GCB DLBCL (D), or all DLBCL (E) (Fisher's exact test). FDR, false discovery rate; FS, frameshift.

domain mutations in HEK IL-4/IL-13 cells, the levels of STAT6-induced secreted embryonic alkaline phosphatase secreted into the cell culture supernatant (Figure 5B) and pSTAT6 (Figure 5C) were increased, independent of IL-4 ligand stimulation, but not upon expression of cytoplasmic IL4R mutations. Consistently, constitutive pSTAT6 activation was confirmed in a B-cell lymphoma–derived cell line (DEV) expressing these extracellular IL4R mutations (Figure 5D). In addition, high expression of *CCL17* and *CD23* (Figure 5E-F) was associated with JAK-STAT activation. In concordance, *CCL17* transcript levels were high in clinical samples with mutations affecting the transmembrane or extracellular domains of IL4R but low in those with cytoplasmic IL4R mutations (supplemental Figure 6). The observation that most nm-PMBLsig⁺ tumors that had WT *IL4R* also showed high *CCL17* transcript levels suggests alternative mechanisms for JAK-STAT activation in these tumors, presumably through mutation of *STAT6*, *DUSP2*, and/or *SOCS1* (Figure 3A).[12] Similar to findings reported by Viganò et al, we confirmed an inverse correlation between JAK-STAT activation (observed as pSTAT6, CD23, and *CCL17* expression) and expression of IL4R protein on the plasma membrane (Figure 5G).[31]

Several gene mutations in nm-PMBLsig⁺ tumors show a pattern of aSHM

Remarkably, all nm-PMBLsig⁺ tumors harbored ≥1 mutation in *SOCS1*. *SOCS1* is a known target for AID-mediated aberrant somatic hypermutation (aSHM) in lymphoma[45,46] and is recurrently

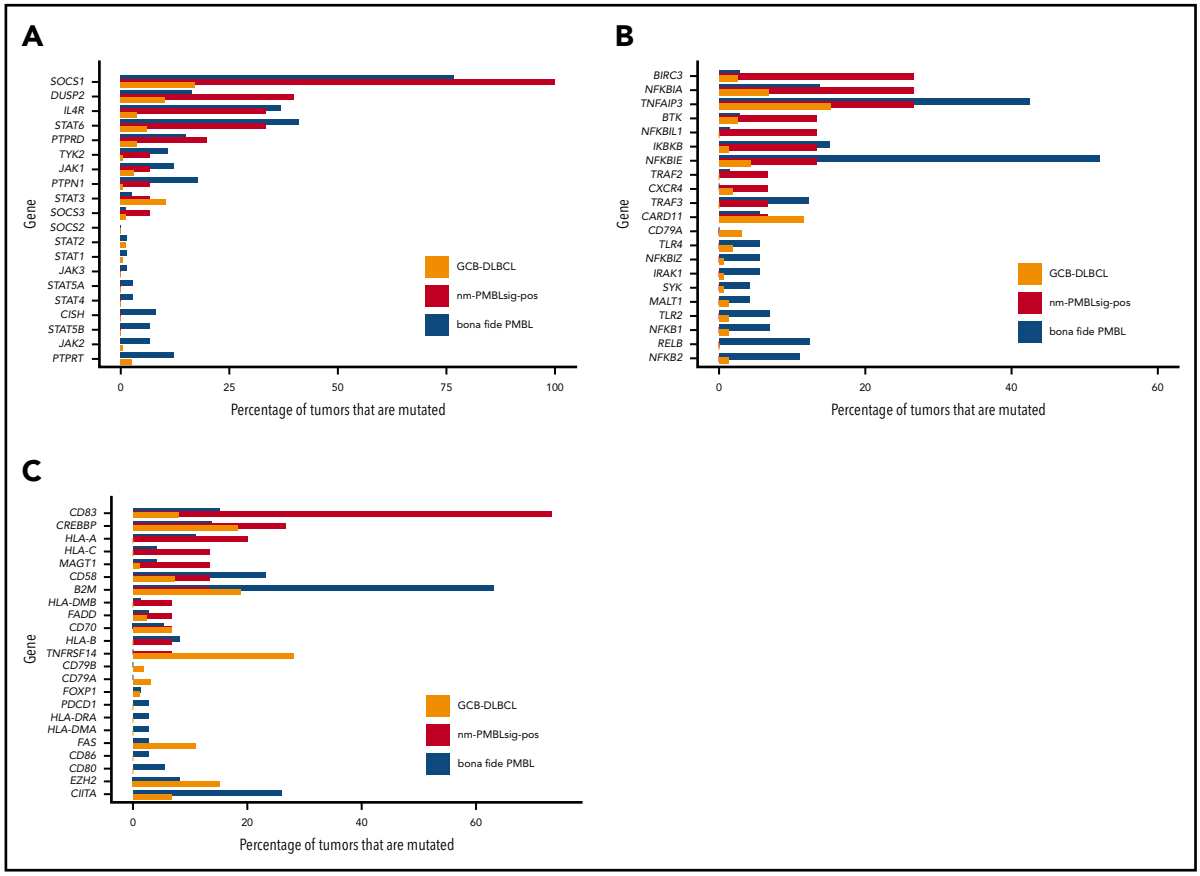

Figure 4. Mutational frequencies affecting genes involved in pathways of interest in GCB DLBCL, nm-PMBLsig$^+$ tumors, and bf-PMBL. (A) JAK-STAT mutations are frequent in both nm-PMBLsig$^+$ tumors and bf-PMBL. Frequencies of mutations affecting genes involved in JAK-STAT signaling are shown for GCB DLBCL, nm-PMBLsig$^+$ tumors, and bf-PMBL. (B) NF-κB signaling mutations are frequent in both nm-PMBLsig$^+$ tumors and bf-PMBL. Frequencies of mutations affecting genes involved in NF-κB signaling are shown for GCB DLBCL, nm-PMBLsig$^+$ tumors, and PMBL. (C) Immune response mutations are common in all 3 subtypes. Frequencies of mutations affecting genes involved in immune response are shown for GCB DLBCL, nm-PMBLsig$^+$ tumors, and bf-PMBL.

mutated in both bf-PMBL[8] and cHL,[47,48] although at lower frequencies. Several other known aSHM targets, including *CD83*, *BCL7A*, *MYC*, *SGK1*, and *PIM1*, were also frequently mutated in nm-PMBLsig$^+$ tumors, and the mutational patterns in these genes were in concordance with aSHM (supplemental Figure 7). Moreover, transcript levels positively correlated with mutational status for these genes, consistent with the concept that SHM preferentially occurs in actively transcribed genes (supplemental Figure 8). While confirming the post-GC origin of nm-PMBLsig$^+$ tumors, further investigation will be required to distinguish aSHM-induced driver mutations from passenger mutations.[49]

Recurrent CN changes in nm-PMBLsig$^+$ tumors

Gain of 9p24, which is frequently observed in bf-PMBL (Figure 6), was identified in a significantly higher fraction of nm-PMBLsig$^+$ tumors compared with GCB DLBCL (33% vs 10%; $P = .03$). 9p24 amplification was associated with increased transcript levels of *JAK2*, *CD274*, and *PDCD1LG2* in nm-PMBLsig$^+$ tumors (supplemental Figure 9).

Besides *JAK2*, several other genes encoding proteins involved in JAK-STAT signaling showed increased CNs specifically in nm-PMBLsig$^+$ samples (supplemental Figure 10). Beyond CN gains of 9p, we observed additional CN changes that add to the shared mutational patterns with bf-PMBL described at the SNV level, most prominently the amplification of the protooncogene *c-REL* located at 2p16.1 (Figure 6). In addition, we identified recurrent CN aberrations that seemed to be specific to nm-PMBLsig$^+$ tumors. These included loss of the immune regulatory gene *CD70* at 19p13.3, which was more frequently observed in nm-PMBLsig$^+$ tumors than in GCB DLBCL (33% vs 10%; $P = .02$; supplemental Figure 11) and not detected as a recurring event in bf-PMBL (Figure 6). Four nm-PMBLsig$^+$ tumors (25%) showed loss of 2q, with a minimally deleted region at 2q11.2 that included 5 genes, including *REV1*. *REV1* encodes a TLS DNA polymerase, the knockdown of which has been shown to sensitize lymphomas to the crosslinking agent cisplatin.[50] *REV1* was deleted in only 1 GCB DLBCL (0.9%), and *REV1* transcript levels were decreased in nm-PMBLsig$^+$ tumors compared with GCB DLBCL (supplemental Figure 12).

Loss and concomitant decrease of transcript levels of *RB1* (13q14.2) and *PTEN* (10q23.31) were found in 16% and 10% of GCB DLBCL samples, respectively, but were not observed in nm-PMBLsig$^+$ samples ($P = .1$ and .3, respectively; supplemental Figures 13 and 14).

Discussion

Here, we have comprehensively characterized the mutational features and clinicopathologic characteristics of patients with de novo DLBCL presenting without evidence of anterior mediastinal

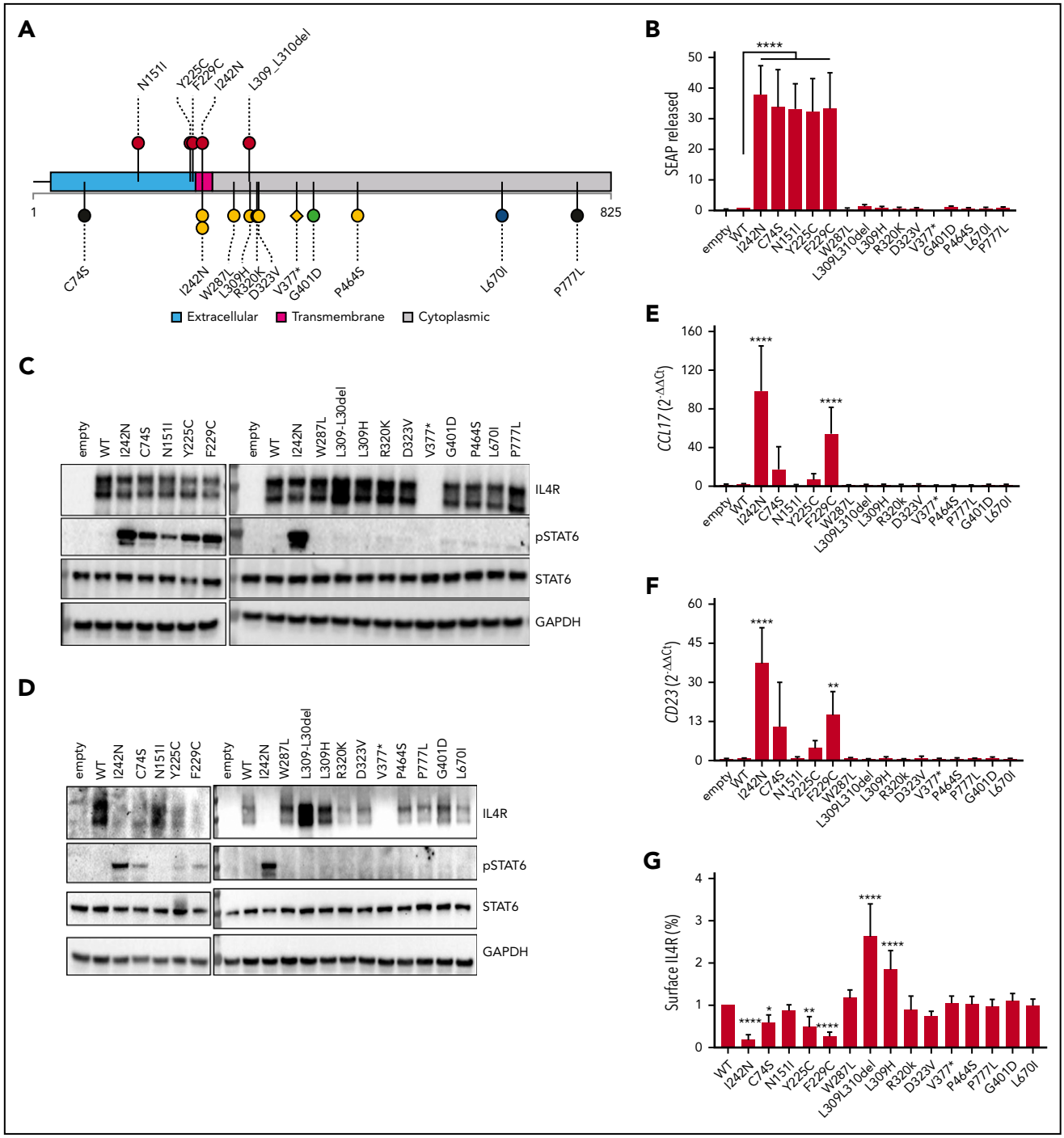

Figure 5. *IL4R* mutations in nm-PMBLsig⁺ tumors induce JAK-STAT activation. (A) Mutational pattern of *IL4R* (UniProtKB-P24394) in nm-PMBLsig⁺ tumors (top) and other DLBCL tumors (bottom) from the BCC cohort specified according to receptor domains (extracellular, transmembrane, or cytoplasmic). Colors and shapes of lollipops represent the DLBCL90 NanoString assay tiered classification of samples (see Figure 1) and type of mutation (circle, missense or in-frame indel; diamond, truncating), respectively. The plot was created using R package TrackViewer (version 1.24.0). (B-G) Ectopic expression of WT IL4R and mutants in HEK Blue IL-4/IL-13 (Invivogen) (B-C) and DEV cells (D-G). (B) Quantification of pSTAT6-dependent expression of secreted embryonic alkaline phosphatase (SEAP) in supernatant. (C-D) Immunoblot for pSTAT6, STAT6, IL4R, and glyceraldehyde-3-phosphate dehydrogenase (GAPDH). (E-F) *CCL17* and *CD23* messenger RNA expression measured by quantitative polymerase chain reaction. (G) IL4R surface expression measured by flow cytometry. Data are means ± standard deviation of 5, 4, 7, and 7 experiments in panels A, E, F, and G, respectively; significance was evaluated using a 1-sample Student *t* test. $*P < .05$, $**P < .01$, $****P < .0001$.

involvement but expressing the PMBL GE signature (nm-PMBLsig⁺). Although previous reports have suggested that these tumors represent nonmediastinal PMBLs,[13] our data indicate that they are clinically distinct from bf-PMBL and have molecular features that distinguish them from other DLBCLs. Identification of these cases from within our large population-based cohort suggests that ~5% of de novo DLBCL, and therefore, ~2% of all B-cell NHLs are nm-PMBLsig⁺. For perspective, these figures suggest an incidence rate similar to or greater than that of bf-PMBL.[51]

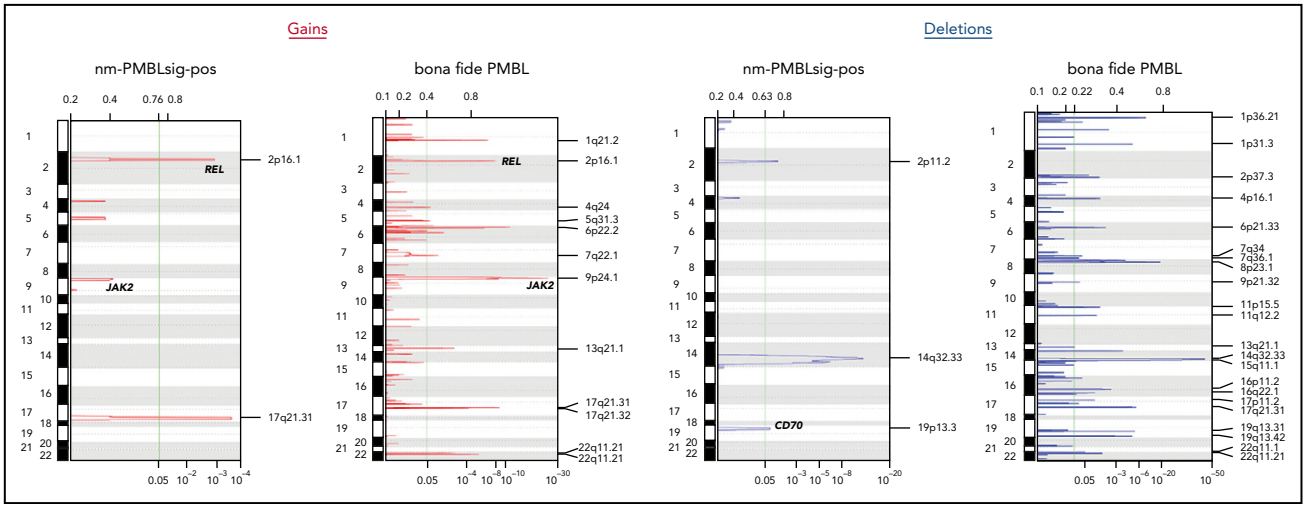

Figure 6. Recurrent CN aberrations in nm-PMBLsig$^+$ tumors and bf-PMBL inferred from WES data. CNs were inferred from WES data using CNVkit; recurrent aberrations were then identified using the *GISTIC* algorithm (see "Methods").

Although the clinical characteristics of nm-PMBLsig$^+$ cases were similar to those of the other DLBCLs within our cohort, they differed considerably with respect to their immunophenotype and mutational landscape. The majority of nm-PMBLsig$^+$ tumors expressed MAL and CD23, proteins typically expressed in bf-PMBL but rarely observed in DLBCL, and all were positive for LMO2 and FAS.

Similar to bf-PMBL,[8,9] these tumors showed frequent aberrations affecting JAK-STAT signaling, including somatic point mutations in *SOCS1*, *STAT6*, *IL4R*, and *DUSP2*, and CN gains involving 9p24.1 that resulted in increased *JAK2*, *CD274*, and *PDCD1LG2* transcript levels. Moreover, we found that mutations affecting *IL4R* were more frequent in nm-PMBLsig$^+$ tumors than in GCB DLBCL and that the pattern of these mutations was also distinct. *IL4R* mutations identified in nm-PMBLsig$^+$ samples predominantly affected the extracellular domain, whereas a majority of *IL4R* mutations in GCB DLBCL affected the cytoplasmic domain. We found that the extracellular domain mutations had the ability to activate JAK-STAT signaling in in vitro models, providing evidence that these mutations contribute to lymphomagenesis in nm-PMBLsig$^+$ tumors. All investigated cytoplasmic *IL4R* mutations lacked this ability, suggesting that a majority of *IL4R* mutations identified in GCB DLBCL represent passenger mutations or contribute to lymphomagenesis through different mechanisms. The observation that cytoplasmic mutations that disrupt the dileucine motif L309-L310 caused an increase in the IL4R protein level (Figure 5C-D) and resulted in sustained IL4R surface receptor expression (Figure 5G) is interesting in this respect. In other receptors, this dileucine motif has been reported to function in clathrin-mediated endocytosis.[52-54] It remains to be investigated whether this is also the case for IL4R and whether L309-L310 mutations contribute to lymphomagenesis by affecting endocytosis of IL4R.

Frequent disruption of immune response was an additional feature that nm-PMBLsig$^+$ tumors shared with bf-PMBL.[8,9] However, other than for the JAK-STAT pathway, the affected genes were different between nm-PMBLsig$^+$ tumors and bf-PMBL, suggesting distinct mechanisms of disruption.

Interestingly, we identified somatic mutations affecting the E3 ubiquitin ligase gene *BIRC3* in 4 of 15 nm-PMBLsig$^+$ tumors. *BIRC3* mutations and translocations are frequent in several hematologic malignancies,[38,55-57] but mutations in DLBCL or bf-PMBL are rare. *BIRC3* has, however, been reported to be involved in recurrently amplified regions in ABC DLBCL.[58]

Our findings are corroborated by 2 recent studies that created new DLBCL classification frameworks by applying computational algorithms to genetic features identified in DLBCL samples. Chapuy et al[59] identified 5 distinct DLBCL subsets using SNVs, translocations, and CN aberrations. A subset of the Chapuy et al cluster 4 DLBCLs showed a mutational landscape similar to that of the nm-PMBLsig$^+$ tumors, with frequent mutations affecting *CD83*, *HIST1H1E*, and *SGK1*. However, *SOCS1* mutations were not reported in this study, because they did not pass MutsigCV filtering thresholds.

Lacy et al[60] used targeted sequencing data to classify DLBCL tumors and identified 6 distinct DLBCL subsets, including a SOCS1/SGK1 group that harbored mutations also found in the nm-PMBLsig$^+$ tumors from our DLBCL cohort, with recurrent mutations affecting *SOCS1*, *SGK1*, *CD83*, *NFKBIA*, *HIST1H1E*, and *STAT3*. This SOCS1/SGK1 group also included a majority of bf-PMBLs (12 of 20) as well as 98 (11.7%) of 839 DLBCL-NOS tumors. As observed for the nm-PMBCLsig$^+$ tumors from our BCC DLBCL cohort, SOCS1/SGK1 DLBCLs did not show pathologic features of PMBL, were not enriched for mediastinal involvement, and were predominantly of GCB origin. However, *BIRC3* mutations were not identified by Lacy et al as a defining feature of SOCS1/SGK1 DLBCL, and therefore, further research is required to assess the role this E3 ligase plays in the pathogenesis of such tumors.

The SOCS1/SGK1 group comprised a higher fraction of the investigated DLBCL cohort than our nm-PMBLsig$^+$ subset (11.7% and 5.0%, respectively). Because DLBCL90 and Lymph3Cx assay results are currently unavailable for the Lacy et al[60] DLBCL cohort, it remains an open question if the observed difference can be explained by between-cohort variation or whether the SOCS1/SGK1

group comprises a phenotypically mixed set of tumors that includes cases negative for the PMBL GE signature.

In addition to somatic mutations, our CN analysis revealed aberrations enriched in nm-PMBLsig$^+$ tumors that could provide potentially novel therapeutic avenues for this subset of DLBCL. For example, patients with nm-PMBLsig$^+$ tumors that show 9p24 gain might benefit from immunotherapy targeting PD-1/PD-L1.[61]

The shared GE pattern, which is the foundation of our study, likely represents a summation of heterogeneous somatic mutations that converge on common pathways and underpin hallmarks shared with bf-PMBL. The strong correlation between somatic mutations and GE phenotypes underscores the robustness of our findings, analogous to the original DLBCL COO classification.[62]

In summary, we have characterized DLBCLs with a PMBL GE signature, showing that they resemble bf-PMBL at the molecular level, with JAK-STAT signaling and immune response being frequently affected in both lymphoma entities. Our data suggest that dysregulation of the latter pathway is established through distinct evolutionary modes that are reflected in differential mutation patterns and anatomic and clinical presentations. With potential implications for classification and diagnostic procedures, this subset of DLBCL that expresses the PMBL signature can readily be identified using the DLBCL90 NanoString assay, emphasizing the value of GE assays in DLBCL subtyping.

Acknowledgments

This study was supported by Program Project Grant funding from the Terry Fox Research Institute (grant 1061), Large Scale Applied Research Project funding from Genome Canada (grant 13124; C.S.), Genome British Columbia (grant 271LYM; C.S.), Canadian Institutes of Health Research (CIHR; grant GP1-155873; C.S.) and the British Columbia Cancer Foundation, and a Foundation Grant from CIHR. C.S. is supported by the Michael Smith Foundation for Health Research, Career Investigator Award. D.W.S. is supported by a Michael Smith Foundation for Health Research, Health Professional Investigator Award. The Centre for Lymphoid Cancer acknowledges the support from the BC Cancer Foundation. E.V. was supported by a fellowship from the Michael Smith Foundation for Health Research.

Authorship

Contribution: G.D. and E.V. designed and performed the research, analyzed and interpreted data, and wrote the manuscript; D.E., C. Sarkozy, A.J., K.T., L.K.H., G.W.S., J.W.C., S.P.S., P.F., A.M., R.D.M., K.J.S., and E.D.H. analyzed and interpreted data; S.S.H. and C.R. analyzed exome sequencing data; E.C., S.B.-N., and B.W.W. performed experiments and interpreted data; R.D.G. provided study material; C. Steidl and D.W.S. supervised, designed the study, and wrote the manuscript; and all authors reviewed the manuscript.

Conflict-of-interest disclosure: C. Steidl has performed consultancy for Seattle Genetics, Curis, Inc, Roche, AbbVie, AstraZeneca, Juno Therapeutics, and Bayer and received research funding from Bristol-Myers Squibb, Epizyme, and Trillium Therapeutics, Inc. C. Steidl, D.W.S., and A.M. are coinventors on a patent ("Method for determining lymphoma type") using NanoString technology. D.W.S. has performed consultancy for AbbVie, AstraZeneca, Celgene, and Janssen and received research funding from Janssen and NanoString Technologies. K.J.S. reports honoraria from Seattle Genetics, Bristol-Myers Squibb, Merck, AbbVie, AstraZeneca, and Gilead; consultancy for Servier; and institutional funds from Roche. J.W.C. has received honoraria from Seattle Genetics and Takeda Pharmaceuticals. E.D.H. has performed consultancy for Cytomx, Seattle Genetics, and Mitenyi and received research funding from AbbVie and Eli Lilly. S.P.S. is a shareholder in Canexia Health Inc. The remaining authors declare no competing financial interests.

ORCID profiles: C.R., 0000-0001-6306-9361; S.B.-N., 0000-0002-2867-4037; J.W.C., 0000-0003-1295-3258; L.K.H., 0000-0002-6413-6586; S.P.S., 0000-0001-6402-523X; P.F., 0000-0001-9364-9391; R.D.M., 0000-0003-2932-7800; K.J.S., 0000-0002-5835-9863; D.W.S., 0000-0002-0435-5947; C. Steidl, 0000-0001-9842-9750.

Correspondence: Christian Steidl, Centre for Lymphoid Cancer, BC Cancer, 675 West 10th Ave, Vancouver, BC V5Z 1L3, Canada; e-mail: csteidl@bccancer.bc.ca.

Footnotes

Submitted 15 June 2020; accepted 12 February 2021; prepublished online on *Blood* First Edition 8 March 2021. DOI 10.1182/blood.2020007683.

*G.D. and E.V. are joint first authors.

†D.W.S. and C. Steidl are joint senior authors.

The data reported in this article have been deposited in the European Genome-phenome Archive (accession number EGAS00001005057).

The online version of this article contains a data supplement.

The publication costs of this article were defrayed in part by page charge payment. Therefore, and solely to indicate this fact, this article is hereby marked "advertisement" in accordance with 18 USC section 1734.

REFERENCES

1. Swerdlow SH, Campo E, Harris NL, et al. WHO classification of tumours of haematopoietic and lymphoid tissues. Revised 4th ed. Lyon, France: IARC Press; 2017.
2. Giulino-Roth L. How I treat primary mediastinal B-cell lymphoma. *Blood*. 2018;132(8):782-790.
3. Barth TF, Leithäuser F, Joos S, Bentz M, Möller P. Mediastinal (thymic) large B-cell lymphoma: where do we stand? *Lancet Oncol*. 2002;3(4):229-234.
4. Isaacson PG, Norton AJ, Addis BJ. The human thymus contains a novel population of B lymphocytes. *Lancet*. 1987;2(8574):1488-1491.
5. Möller P, Lämmler B, Eberlein-Gonska M, et al. Primary mediastinal clear cell lymphoma of B-cell type. *Virchows Arch A Pathol Anat Histopathol*. 1986;409(1):79-92.
6. Rosenwald A, Wright G, Leroy K, et al. Molecular diagnosis of primary mediastinal B cell lymphoma identifies a clinically favorable subgroup of diffuse large B cell lymphoma related to Hodgkin lymphoma. *J Exp Med*. 2003;198(6):851-862.
7. Savage KJ, Monti S, Kutok JL, et al. The molecular signature of mediastinal large B-cell lymphoma differs from that of other diffuse large B-cell lymphomas and shares features with classical Hodgkin lymphoma. *Blood*. 2003;102(12):3871-3879.
8. Mottok A, Hung SS, Chavez EA, et al. Integrative genomic analysis identifies key pathogenic mechanisms in primary mediastinal large B-cell lymphoma. *Blood*. 2019;134(10):802-813.
9. Chapuy B, Stewart C, Dunford AJ, et al. Genomic analyses of PMBL reveal new drivers and mechanisms of sensitivity to PD-1 blockade. *Blood*. 2019;134(26):2369-2382.
10. Sarkozy C, Copie-Bergman C, Damotte D, et al. Gray-zone lymphoma between cHL and large B-cell lymphoma: a histopathologic series from the LYSA. *Am J Surg Pathol*. 2019;43(3):341-351.
11. Mottok A, Wright G, Rosenwald A, et al. Molecular classification of primary mediastinal large B-cell lymphoma using routinely available tissue specimens. *Blood*. 2018;132(22):2401-2405.
12. Dubois S, Viailly PJ, Mareschal S, et al. Next-generation sequencing in diffuse large B-cell

lymphoma highlights molecular divergence and therapeutic opportunities: a LYSA study. *Clin Cancer Res*. 2016;22(12):2919-2928.

13. Yuan J, Wright G, Rosenwald A, et al; Lymphoma Leukemia Molecular Profiling Project (LLMPP). Identification of primary mediastinal large B-cell lymphoma at nonmediastinal sites by gene expression profiling. *Am J Surg Pathol*. 2015;39(10):1322-1330.
14. Ennishi D, Mottok A, Ben-Neriah S, et al. Genetic profiling of *MYC* and *BCL2* in diffuse large B-cell lymphoma determines cell-of-origin-specific clinical impact. *Blood*. 2017; 129(20):2760-2770.
15. Arthur SE, Jiang A, Grande BM, et al. Genome-wide discovery of somatic regulatory variants in diffuse large B-cell lymphoma. *Nat Commun*. 2018;9(1):4001.
16. Ennishi D, Jiang A, Boyle M, et al. Double-hit gene expression signature defines a distinct subgroup of germinal center B-cell-like diffuse large B-cell lymphoma. *J Clin Oncol*. 2019; 37(3):190-201.
17. Wright G, Tan B, Rosenwald A, Hurt EH, Wiestner A, Staudt LM. A gene expression-based method to diagnose clinically distinct subgroups of diffuse large B cell lymphoma. *Proc Natl Acad Sci USA*. 2003;100(17): 9991-9996.
18. Li H, Durbin R. Fast and accurate long-read alignment with Burrows-Wheeler transform. *Bioinformatics*. 2010;26(5):589-595.
19. Koboldt DC, Zhang Q, Larson DE, et al. VarScan 2: somatic mutation and copy number alteration discovery in cancer by exome sequencing. *Genome Res*. 2012;22(3):568-576.
20. Saunders CT, Wong WS, Swamy S, Becq J, Murray LJ, Cheetham RK. Strelka: accurate somatic small-variant calling from sequenced tumor-normal sample pairs. *Bioinformatics*. 2012;28(14):1811-1817.
21. Cibulskis K, Lawrence MS, Carter SL, et al. Sensitive detection of somatic point mutations in impure and heterogeneous cancer samples. *Nat Biotechnol*. 2013;31(3):213-219.
22. Cingolani P, Platts A, Wang L, et al. A program for annotating and predicting the effects of single nucleotide polymorphisms, SnpEff: SNPs in the genome of Drosophila melanogaster strain w1118; iso-2; iso-3. *Fly (Austin)*. 2012;6(2):80-92.
23. Sherry ST, Ward MH, Kholodov M, et al. dbSNP: the NCBI database of genetic variation. *Nucleic Acids Res*. 2001;29(1):308-311.
24. Tate JG, Bamford S, Jubb HC, et al. COSMIC: the Catalogue Of Somatic Mutations In Cancer. *Nucleic Acids Res*. 2019;47(D1): D941-D947.
25. Schmitz R, Wright GW, Huang DW, et al. Genetics and pathogenesis of diffuse large B-cell lymphoma. *N Engl J Med*. 2018;378(15): 1396-1407.
26. Ennishi D, Takata K, Béguelin W, et al. Molecular and genetic characterization of MHC deficiency identifies EZH2 as therapeutic target for enhancing immune recognition. *Cancer Discov*. 2019;9(4):546-563.
27. Anders S, Pyl PT, Huber W. HTSeq—a Python framework to work with high-throughput sequencing data. *Bioinformatics*. 2015;31(2): 166-169.
28. Robinson MD, McCarthy DJ, Smyth GK. edgeR: a Bioconductor package for differential expression analysis of digital gene expression data. *Bioinformatics*. 2010;26(1): 139-140.
29. Talevich E, Shain AH, Botton T, Bastian BC. CNVkit: genome-wide copy number detection and visualization from targeted DNA sequencing. *PLOS Comput Biol*. 2016;12(4): e1004873.
30. Mermel CH, Schumacher SE, Hill B, Meyerson ML, Beroukhim R, Getz G. GISTIC2.0 facilitates sensitive and confident localization of the targets of focal somatic copy-number alteration in human cancers. *Genome Biol*. 2011;12(4):R41.
31. Viganò E, Gunawardana J, Mottok A, et al. Somatic IL4R mutations in primary mediastinal large B-cell lymphoma lead to constitutive JAK-STAT signaling activation. *Blood*. 2018; 131(18):2036-2046.
32. Lenz G, Wright G, Dave SS, et al; Lymphoma/Leukemia Molecular Profiling Project. Stromal gene signatures in large-B-cell lymphomas. *N Engl J Med*. 2008;359(22):2313-2323.
33. Scott DW, Wright GW, Williams PM, et al. Determining cell-of-origin subtypes of diffuse large B-cell lymphoma using gene expression in formalin-fixed paraffin-embedded tissue. *Blood*. 2014;123(8):1214-1217.
34. Bledsoe JR, Redd RA, Hasserjian RP, et al. The immunophenotypic spectrum of primary mediastinal large B-cell lymphoma reveals prognostic biomarkers associated with outcome. *Am J Hematol*. 2016;91(10): E436-E441.
35. Gentry M, Bodo J, Durkin L, Hsi ED. Performance of a commercially available mal antibody in the diagnosis of primary mediastinal large B-cell lymphoma. *Am J Surg Pathol*. 2017;41(2):189-194.
36. Hans CP, Weisenburger DD, Greiner TC, et al. Confirmation of the molecular classification of diffuse large B-cell lymphoma by immunohistochemistry using a tissue microarray. *Blood*. 2004;103(1):275-282.
37. Liston P, Roy N, Tamai K, et al. Suppression of apoptosis in mammalian cells by NAIP and a related family of IAP genes. *Nature*. 1996; 379(6563):349-353.
38. Rahal R, Frick M, Romero R, et al. Pharmacological and genomic profiling identifies NF-κB-targeted treatment strategies for mantle cell lymphoma. *Nat Med*. 2014;20(1):87-92.
39. Li X, Yang Y, Ashwell JD. TNF-RII and c-IAP1 mediate ubiquitination and degradation of TRAF2. *Nature*. 2002;416(6878):345-347.
40. Hu S, Du MQ, Park SM, et al. cIAP2 is a ubiquitin protein ligase for BCL10 and is dysregulated in mucosa-associated lymphoid tissue lymphomas. *J Clin Invest*. 2006;116(1): 174-181.
41. Lopez J, John SW, Tenev T, et al. CARD-mediated autoinhibition of cIAP1's E3 ligase activity suppresses cell proliferation and migration. *Mol Cell*. 2011;42(5):569-583.
42. Mansouri L, Noerenberg D, Young E, et al. Frequent NFKBIE deletions are associated with poor outcome in primary mediastinal B-cell lymphoma. *Blood*. 2016;128(23): 2666-2670.
43. Challa-Malladi M, Lieu YK, Califano O, et al. Combined genetic inactivation of β2-Microglobulin and CD58 reveals frequent escape from immune recognition in diffuse large B cell lymphoma. *Cancer Cell*. 2011; 20(6):728-740.
44. Steidl C, Shah SP, Woolcock BW, et al. MHC class II transactivator CIITA is a recurrent gene fusion partner in lymphoid cancers. *Nature*. 2011;471(7338):377-381.
45. Khodabakhshi AH, Morin RD, Fejes AP, et al. Recurrent targets of aberrant somatic hypermutation in lymphoma. *Oncotarget*. 2012; 3(11):1308-1319.
46. Morin RD, Mungall K, Pleasance E, et al. Mutational and structural analysis of diffuse large B-cell lymphoma using whole-genome sequencing. *Blood*. 2013;122(7):1256-1265.
47. Weniger MA, Melzner I, Menz CK, et al. Mutations of the tumor suppressor gene SOCS-1 in classical Hodgkin lymphoma are frequent and associated with nuclear phospho-STAT5 accumulation. *Oncogene*. 2006;25(18):2679-2684.
48. Tiacci E, Ladewig E, Schiavoni G, et al. Pervasive mutations of JAK-STAT pathway genes in classical Hodgkin lymphoma. *Blood*. 2018;131(22):2454-2465.
49. Mellert K, Martin M, Lennerz JK, et al. The impact of SOCS1 mutations in diffuse large B-cell lymphoma. *Br J Haematol*. 2019;187(5): 627-637.
50. Xie K, Doles J, Hemann MT, Walker GC. Error-prone translesion synthesis mediates acquired chemoresistance. *Proc Natl Acad Sci USA*. 2010;107(48):20792-20797.
51. Teras LR, DeSantis CE, Cerhan JR, Morton LM, Jemal A, Flowers CR. 2016 US lymphoid malignancy statistics by World Health Organization subtypes. *CA Cancer J Clin*. 2016; 66(6):443-459.
52. Ehrlich M, Shmuely A, Henis YI. A single internalization signal from the di-leucine family is critical for constitutive endocytosis of the type II TGF-beta receptor. *J Cell Sci*. 2001; 114(Pt 9):1777-1786.
53. Huang L, Kirschke CP. A di-leucine sorting signal in ZIP1 (SLC39A1) mediates endocytosis of the protein. *FEBS J*. 2007;274(15): 3986-3997.
54. Kozik P, Francis RW, Seaman MN, Robinson MS. A screen for endocytic motifs. *Traffic*. 2010;11(6):843-855.
55. Dierlamm J, Baens M, Wlodarska I, et al. The apoptosis inhibitor gene API2 and a novel 18q gene, MLT, are recurrently rearranged in the t(11;18)(q21;q21) associated with mucosa-associated lymphoid tissue lymphomas. *Blood*. 1999;93(11):3601-3609.
56. Diop F, Moia R, Favini C, et al. Biological and clinical implications of *BIRC3* mutations in chronic lymphocytic leukemia. *Haematologica*. 2020;105(2):448-456.

57. Rossi D, Deaglio S, Dominguez-Sola D, et al. Alteration of BIRC3 and multiple other NF-κB pathway genes in splenic marginal zone lymphoma. *Blood*. 2011;118(18):4930-4934.

58. Yang Y, Kelly P, Shaffer AL III, et al. Targeting non-proteolytic protein ubiquitination for the treatment of diffuse large B cell lymphoma. *Cancer Cell*. 2016;29(4):494-507.

59. Chapuy B, Stewart C, Dunford AJ, et al. Molecular subtypes of diffuse large B cell lymphoma are associated with distinct pathogenic mechanisms and outcomes [published corrections appear in *Nat Med*. 2018;24(8):1290-1291; *Nat Med*. 2018;24(8):1292]. *Nat Med*. 2018;24(5):679-690.

60. Lacy SE, Barrans SL, Beer PA, et al. Targeted sequencing in DLBCL, molecular subtypes, and outcomes: a Haematological Malignancy Research Network report. *Blood*. 2020;135(20):1759-1771.

61. Zinzani PL, Santoro A, Gritti G, et al. Nivolumab combined with brentuximab vedotin for relapsed/refractory primary mediastinal large B-cell lymphoma: efficacy and safety from the phase II CheckMate 436 study. *J Clin Oncol*. 2019;37(33):3081-3089.

62. Lenz G, Wright GW, Emre NC, et al. Molecular subtypes of diffuse large B-cell lymphoma arise by distinct genetic pathways. *Proc Natl Acad Sci USA*. 2008;105(36):13520-13525.